Published in final edited form as:
*Mol Cell*. 2012 July 13; 47(1): 50–60. doi:10.1016/j.molcel.2012.04.028.

# Atl1 regulates choice between global genome and transcription-coupled repair of $O^6$-alkylguanines

**Vitaly F. Latypov**[1], **Julie L. Tubbs**[2], **Amanda J. Watson**[1], **Andrew S. Marriott**[1], **Gail McGown**[1], **Mary Thorncroft**[1], **Oliver J. Wilkinson**[3], **Pattama Senthong**[1,5], **Amna Butt**[1], **Andrew S. Arvai**[2], **Christopher L. Millington**[3], **Andrew C. Povey**[5], **David M. Williams**[3], **Mauro F. Santibanez-Koref**[4], **John A. Tainer**[2,**], and **Geoffrey P. Margison**[1,*]

[1]Cancer Research UK Carcinogenesis Group, Paterson Institute for Cancer Research, University of Manchester, Manchester, M20 4BX, UK

[2]Skaggs Institute for Chemical Biology and Department of Molecular Biology, the Scripps Research Institute, La Jolla, California, 92037, USA

[3]Centre for Chemical Biology Department of Chemistry, Krebs Institute, University of Sheffield, Sheffield, S3 7HF, UK

[4]Institute of Human Genetics, University of Newcastle, Newcastle, NE1 3BZ, UK

[5]Centre for Occupational and Environmental Health, Faculty of Medical and Human Sciences, University of Manchester, Manchester, M13 9PL, UK

## SUMMARY

Nucleotide excision repair (NER) has long been known to remove DNA lesions induced by chemical carcinogens, and the molecular mechanism has been partially elucidated. Here we demonstrate that in *S.pombe* a DNA recognition protein, alkyltransferase-like 1 (Atl1), can play a pivotal role in selecting a specific NER pathway dependent on the nature of the DNA modification. The relative ease of dissociation of Atl1 from DNA containing small $O^6$-alkylguanines allows accurate completion of global genome repair (GGR), whereas strong Atl1 binding to bulky $O^6$-alkylguanines blocks GGR, stalls the transcription machinery and diverts the damage to transcription-coupled repair. Our findings redraw the initial stages of the NER process in those organisms that express an alkyltransferase-like gene and raise the question of whether or not $O^6$-alkylguanine lesions that are poor substrates for the alkyltransferase proteins in higher eukaryotes might, by analogy, signal such lesions for repair by NER.



*Corresponding author: gmargison@picr.man.ac.uk. **Co-corresponding author: jat@scripps.edu.

The authors declare that there are no conflicts of interest.

**Accession Numbers**

Atomic coordinates and structure factors have been deposited in the Protein Data Bank under accession codes 4ENJ (Atl1:$O^6$-HOEtG), 4ENK (Atl1:$O^6$-PrG), 4ENM (Atl1:$O^6$-BnG), and 4ENN (Atl1:$O^6$-CMG).

Further details for all these analyses are in the Supplementary Methods.

## INTRODUCTION

Alkylating agents are a diverse class of genotoxins that elicit a wide range of adverse biological effects in living organisms. Alkylation of the $O^6$-position of guanine in DNA, if not repaired before DNA replication, can give rise to transition mutations and recombination events in surviving cells, or can be cytotoxic. In the case of $O^6$-methylguanine ($O^6$-MeG), toxicity is due to the action of the post-replication mismatch repair (MMR) system. $O^6$-alkylguanines ($O^6$-alkG) in DNA have long been known to be substrates for $O^6$-alkylguanine-DNA alkyltransferases (AGTs), proteins that transfer the alkyl group to a cysteine residue in the highly conserved active site PCHRV/I motif. AGTs are thereby able to protect cells and organisms against the biological effects of alkylating agents (Margison et al., 2002).

The alkyltransferase-like (ATL) proteins are a recently-discovered family that exists in prokaryotes and lower eukaryotes (Margison et al., 2003). They have amino acid sequence motifs that resemble those found in AGTs, but the cysteine residue in the binding site motif is replaced, usually by tryptophan. We previously demonstrated that ATL proteins from *E. coli* (eATL) and *S. pombe* (Atl1) lack the ability to carry out repair by alkyl group transfer or removal, and that they did not display the glycosylase or endonuclease activity that is characteristic of the base excision repair (BER) pathway (Pearson et al., 2005; Pearson et al., 2006). However, deletion of the Atl1-encoding gene in *S. pombe* increased its sensitivity to the toxic effects of a number of alkylating agents (Margison et al., 2007; Pearson et al., 2006) and the mutagenic effects of the methylating agent, *N*-methyl-*N*′-nitro-*N*-nitrosoguanidine (MNNG) (Tubbs et al., 2009). Thus Atl1 is involved in protecting *S. pombe* against the biological effects of alkylating agents.

Crystal structures of Atl1 bound to oligodeoxyribonucleotide (ODN) containing $O^6$-MeG or $O^6$-(4-oxo-4-(3-pyridyl)butyl)guanine ($O^6$-PobG) have shown that the alkylated guanine is rotated into a binding pocket and that there is considerable DNA bending (45°). Previous genetic analyses showed that *atl1* is epistatic with *rad13* (human XPG) and *swi10* (human ERCC1) (Tubbs et al., 2009). Together, these results suggest that Atl1 binding to $O^6$-alkylguanines results in structural changes in DNA that presents these lesions to the nucleotide excision repair (NER) pathway. However, prior to the current study, it remained unknown if the global genome repair (GGR) or transcription coupled repair (TCR) branches of NER were engaged by Atl1.

In the present report, we have carried out epistasis and cell cycle analysis of the interactions between *atl1* and GGR and TCR genes. We show that Atl1 is vital for initiating the processing of damage produced by simple alkylating agents principally *via* the GGR pathway. In contrast, Atl1 exacerbates the toxicity of lesions generated by bulky alkylating agents in NER-defective cells. This occurs more extensively in cells defective in TCR, probably as a direct or indirect consequence of stalling at replication forks. The crystal structures and interaction kinetics of Atl1 with a range of $O^6$-alkylguanines of different complexity suggest that different affinities of Atl1 for simple and bulky DNA lesions determine which pathway is engaged in lesion processing.

## RESULTS

### NER pathway selection by Atl1 is alkylating agent-dependent

The processing of DNA lesions by NER involves damage recognition, repair complex assembly and damage removal. Broadly, in humans, damage in transcribed genes can stall transcription complexes resulting in CSB-mediated TCR while damage elsewhere in the genome is recognised by the DDB1–DDB2 and XPC-hHR23b complexes that initiate GGR.

Both pathways subsequently involve the transcription complex TFIIH, XPA and RPA, the elimination of the damage by the endonucleases XPF and XPG and the restoration of the DNA by polymerase and ligase.

In S.pombe, standard "spot" and clonogenic assays showed that deletion of *atl1* or deletions of the GGR genes, *rhp23, rhp14, swi10, rhp41*, and *rhp7* (human HR23B, XPA, ERCC1, XPC and DDB2) sensitised cells to MNNG, whereas deletions of the TCR gene, *rhp26* (human CSB) or the homologous recombination (HR) gene *rad50* (human Rad50), did not (Figure 1A, 2). We also demonstrated that *atl1* is epistatic with *rhp23, rhp41* and *swi10* but additional deletion of *atl1* increased MNNG toxicity in the *rhp7* and *rhp14* deletants (Figure 1B, 2A–D). The very high sensitivity of the *rhp7 rhp26* double deletant strain (Figure 2E) strain suggests that TCR can partially compensate for GGR deficiency when cells are exposed to MNNG. The *atl1 rad50* double deletant was also extremely sensitive (Figure 2F), indicating that HR is a backup pathway in the absence of Atl1.

The *atl1* and *swi10* deletants were not sensitive to another commonly used methylating agent methyl methanesulfonate (MMS, Figure S1), which generates relatively low levels of $O^6$-MeG in DNA (Beranek, 1990; Singer and Grunberger, 1983). This agrees with the suggestion that $O^6$-MeG is the principal lethal lesion induced by MNNG. To confirm this, we determined $O^6$-MeG levels in DNA extracted from various strains following a short exposure to MNNG. In WT, *rhp26*Δ and *rad50*Δ cells there was a rapid decrease in $O^6$-MeG levels with time (Figure 2G) with more than 50% repair (~1200 $O^6$-MeG residues removed) within 40 min. In contrast, there was little or no removal of $O^6$-MeG in the *swi10*, *rad13*, *rhp23*, *rhp14* and *rhp41* deletants up to 80 min after treatment. There was also some repair of $O^6$-MeG in the *rhp7* deletant, but to a much lesser extent than in the WT strain (Figure 2G). $O^6$-MeG therefore persisted in the DNA of those deletants that displayed increased sensitivity to MNNG but was removed from the DNA of the resistant strains.

We then examined sensitivity of WT strain and *atl1*, *rhp7, rhp23, rhp14, rhp26, swi10* and *rad50* deletants to the ethylating agent *N*-ethyl-*N*-*nitrosourea* (ENU) and two agents that introduce bulkier lesions into DNA i.e. N-butyl-*N*′-nitro-*N*-nitrosoguanidine (BNNG) and *N*-benzyl-*N*-nitrosourea (BzNU). Using spot assays, we were intrigued to find that while deletion of *atl1* increased sensitivity to ENU, it had no effect on sensitivity to BNNG or BzNU (Figure 1B). Moreover, while deletion of the TCR gene *rhp26* had no effect on sensitivity to ENU it extensively increased sensitivity to BNNG and BzNU. Deletion of the GGR genes *rhp23*, *rhp14* and *swi10* significantly increased the toxicity to all alkylating agents whereas deletion of *rhp7* had only marginal effects on sensitivity in all cases (Figure 1A).

Our earlier investigations had suggested that Atl1 would bind to a range of $O^6$-alkylguanines in DNA (Pearson et al., 2006), so the lack of any effect of *atl1* deletion on sensitivity to the bulkier alkylating agents was unexpected. Investigating the basis of this in double deletants, we found that deletion of *atl1* complemented the sensitivity of all NER-deficient strains, but particularly the *rhp26* deletant, to BNNG and BzNU (Figure 1B). The effect of *atl1* deletion on the sensitivity to BNNG and BzNU was only observed in the *rad50*Δ strain, indicating that the HR pathway compensates for the absence of Atl1.

### Atl1 binding delays chromosome replication after high dose MNNG or low dose BzNU

To examine if Atl1 binding to $O^6$-alkylguanine residues might result in a DNA replication block, we used flow cytometry to measure S-phase progression after release of G1-arrested *cdc10-M17* following brief exposure to MNNG or BzNU. The shift of the histogram peaks over time (Figure 3A and C) was used to quantitate progression through S-phase (Figure 3B and D). At low doses of MNNG, there was no indication of delayed progression in WT or

*atl1*, *swi10* or *rhp26* deletants (data not shown). However, after a very high dose of MNNG there was an additional delay of ~60 min in WT cells. This delay was essentially attributable to Atl1 since the progression profile after MNNG- treatment of the *atl1* deletant overlapped with that of the untreated WT (Figure 3B).

To investigate G1-arrest by BzNU, we used doses that resulted in ~27% cell survival: higher doses caused complete suppression of replication (data not shown). We observed a substantial (~80 min) delay after releasing the replication block in WT cells treated with BzNU. Deletion of *atl1* shortened this delay by ~40 min. These data suggest that the delay in replication onset is, at least in part, Atl1-mediated. Deletions of the *rhp26* and *swi10* genes had little or no impact on the delay of replication onset in untreated cells, but caused a very substantial delay in BzNU treated cells. Again, deletion of the *atl1* gene shortened the S-phase delay in both of these deletants but the extent of the shortening was much more substantial in the *rhp26* deletant strain (Figure 3C).

## *O*$^6$-methylguanine is less toxic than *O*$^6$-benzylguanine

To compare the relative toxic effects of $O^6$-MeG and $O^6$-BnG in chromosomal DNA, we treated *S. pombe* wild-type cells with two concentrations each of MNNG and BzNU which resulted in ~60% and ~30% survival. We found ~6030 and ~8030 $O^6$-MeGs and ~185 and ~206 $O^6$-BnGs per cell respectively (Table S3), suggesting that $O^6$-BnG is approximately 20 times more toxic than $O^6$-MeG: on average one $O^6$-BnG per 72000 bases will kill ~60% of cells.

## Structural analysis of Atl1 bound to *O*$^6$-alkylguanine-containing ODN duplexes

To determine if the above observations might reflect differences in Atl1-$O^6$-alkylguanine interactions, we initially used electrophoretic mobility shift assays (EMSA) to assess binding to ODN duplexes containing a range of $O^6$-alkylguanines. No shift was seen with the control (G-containing) ODN, but ODN containing single $O^6$-methyl (Me), carboxymethyl (CM), -ethyl (Et), -hydroxyethyl (HOEt), -propyl (Pr), -butyl (Bu) -benzyl (Bn), -pyridyloxobutyl (Pob) or -4-bromothenyl (BT) guanine residues were shifted (Figure 4A). These ODN shifts were ablated by proteinase K digestion of the Atl1-ODN complex and no shifts were seen with the non-DNA binding protein maltose-binding protein (MBP) (Figure 4B and 4S).

We then solved crystal structures for Atl1 in complex with duplex ODNs containing $O^6$-HOEtG, $O^6$-PrG, $O^6$-BnG and $O^6$-CMG (Figure 5C–F, Table 1). All complexes crystallized in space group $P6_122$ or $P4_12_12$ with very similar overall structures (Figure 5A). For each lesion, the damaged base is rotated out of the DNA helix and into the Atl1 binding pocket, with Arg 39 donating a hydrogen bond to the orphaned cytosine to stabilize the extrahelical DNA conformation. Also, in all cases, the DNA is bent ~45°. These observations are consistent with previous crystal structures of Atl1 in complex with ODN duplexes of the same sequence containing $O^6$-MeG or $O^6$-PobG (*6*). $O^6$-HOEtG, $O^6$-PrG, $O^6$-BnG and $O^6$-CMG adducts fit within the predominantly hydrophobic Atl1 binding pocket, which is capped by Pro 50, without significant rearrangement of side chains for surrounding amino acid residues. The predominant interactions between the hydroxyethyl, propyl, and benzyl side chains of the adducts and the amino acid side chains in the interior of the Atl1 binding pocket are hydrophobic in nature (Figure 5B). Additional hydrogen bonds with neighbouring carbonyl oxygen atoms stabilize the HOEtG and CMG adducts. Unable to make similar interactions, the propyl and benzyl groups show increased mobility as signified by higher B factors and reduced electron density for these adducts. The higher mobility of propyl and benzyl groups may facilitate their alignment with the hydrophobic interior of the binding pocket and contribute to the high affinity of Atl1 for these alkyl groups. Together,

these results indicate that a variety of lesions can be accommodated in the Atl1 binding pocket. Larger groups make stronger hydrophobic interactions than smaller groups or groups that can establish weaker hydrogen bonding interactions, suggesting the larger lesions may bind Atl1 more tightly. Since this might influence the downstream interactions that determine how the lesion is processed, we undertook quantitative assessment of Atl1 binding using lesion-containing ODN duplexes.

### The affinity of Atl1 for $O^6$-alkylguanines increases with the size of the alkyl group

Binding of Atl1 to control or modified duplex ODN that had been immobilized via a 5′-terminal biotin to SA-coated microtitre plates was quantified by ELISA. Typical Atl1 concentration-dependence curves and extrapolated $K_D$ values are shown in Figure 6A and B respectively. No Atl1 binding was seen using control (G-containing) duplex ODN (data not shown) and its affinity for duplex ODNs containing $O^6$-MeG or $O^6$-CMG was similar but less than for the other duplexes, the most potent of which contained $O^6$-BuG, $O^6$-BnG, $O^6$-PobG and $O^6$-BTG: binding to $O^6$-EtG showed an intermediate value.

We next used surface plasmon resonance (SPR) to quantify the binding of Atl1 to, and dissociation from, control or modified duplex ODN. Sensorgrams (Figure 6C) indicated similarities in association ("on") rates ($k_a$ values 0.21–0.45 $M^{-1}sec^{-1} \times 10^7$), but substantial differences in dissociation ("off") rates ($k_d$ values 0.14 – 3.13 $sec^{-1} \times 10^{-3}$ (Figure 6D). The resulting $K_D$ values ranged over more than one order of magnitude (0.05–0.91 nM; Figure 6D) and clearly demonstrated that the affinities of Atl1 for bulky $O^6$-alkylguanines (0.05–0.1 nM) were substantially higher than for the simpler lesions (0.5–0.91 nM).

## DISCUSSION

The NER pathways have not been extensively investigated in *S. pombe*, but by analogy with the systems in *S. cerevisiae* and higher eukaryotes, are likely to be differentiated by the lesion recognition step. In GGR, DNA damage is detected throughout the genome of *S. cerevisiae* by the RAD7-RAD16-Ecl1-Cullin3 (NEF4) complex sharing certain functional similarities with human DDB1-DDB2-Roc1-cullin4 complex (Fuss and Tainer, 2011; Prakash and Prakash, 2000; Reed, 2011). The equivalent complex in *S. pombe* is *rhp7-rhp16*-based (Lombaerts et al., 1999). In *S. cerevisiae,* the initial step is followed by the recruitment of the RAD4-RAD23-Rad33 complex (Rhp41-Rhp23-Cdc31 in *S. pombe* and XPC-hHR23b-centrin-2 in *H. sapiens*, (den Dulk et al., 2008; Lombaerts et al., 2000; Marti et al., 2003; Nouspikel, 2009; Paoletti et al., 2003). In TCR, damage in the transcribed strand stalls the transcription complex and CSB (RAD26 in *S. cerevisiae* and Rhp26 in *S. pombe*) initiates the repair process (Fousteri and Mullenders, 2008; Yasuhira et al., 1999). Subsequently the two pathways merge with the recruitment of transcription factor II H (TFIIH) and various other factors that eventually result in the excision of the lesion within a short fragment (23–27 nucleotides) of DNA (reviewed in (Fousteri and Mullenders, 2008; Fuss and Tainer, 2011; Nouspikel, 2009)).

### Atl1 protects against the toxic effects of MNNG

The present results indicate that in *S.pombe*, protection against the lethal effects of MNNG requires the GGR-specific genes *rhp7*, *rhp23* and *rhp41*, but not the TCR-specific gene *rhp26*, the BER gene *apn2* (Figure S1) or the HR gene *rad50*. We also show that the lesion predominantly responsible for killing by MNNG is $O^6$-MeG.

Atl1 binds strongly to DNA containing $O^6$-MeG *in vitro*, and might thus be expected to fulfil the role of the Rhp7 complex (see above). However, the *rhp7* deletant was moderately sensitive to MNNG and impaired in its ability to remove $O^6$-MeG. Thus Rhp7 seems to be

at least partially involved in these processes. In human cells, what seems to be important for the subsequent step in NER is that opposite the damaged bases there are unpaired bases to which the XPC-hHR23b-centrin-2 complex binds (Min and Pavletich, 2007; Nouspikel, 2009). Our crystal structures show that Atl1 binding to $O^6$-MeG generates a single unpaired C in the opposite strand, and while this might be anticipated to be capable of recruiting the Rhp41 complex, there would then be no obvious role for the Rhp7 complex. It therefore seems reasonable to propose a model (Figure 7) in which, for the majority of $O^6$-MeG lesions, the Rhp7 complex facilitates Rhp41 binding via an interaction with the Atl1- lesion complex, possibly involving chromatin remodelling, or displacement of Atl1, and hence generating a more extensive DNA melting region for Rhp41 complex binding.

The toxicity of $O^6$-MeG is likely to be a consequence of replication of $O^6$-MeG-containing DNA giving rise to $O^6$-MeG:T mispairs. These are recognised by the post replication MMR system, which results in a reiterative cycle of resynthesis and degradation of the T-containing strand (Hickman and Samson, 2004). After a further round of replication the gapped duplex results in DNA double-strand breaks (DSBs) that can be processed by recombination repair or give rise to lethality. That the *atl1 rad50* double deletant was extremely sensitive to MNNG toxicity (Figure 1 and 2F) confirms that the toxic effects of MNNG can be rescued by the HR machinery.

After high doses of MNNG, the abundance of Rhp7/Rhp16 and Rhp41/Rhp23 complexes may not be sufficient to initiate GGR at all DNA lesions and consequently some Atl1-$O^6$-MeG complexes may persist long enough to block DNA replication, either directly or by stalling RNA polymerase II. Indeed, after exposure of WT cells to high doses of MNNG, we observed substantial delay in S-phase progression and degradation of the RNA polymerase II large subunit, Rpb1 that was completely dependent on Atl1 (Figure 3A and B, S2). This indicates that Atl1-$O^6$-MeG complexes can stall RNA polymerase II: the stalled transcription complex probably then stalls DNA replication.

## Processing of $O^6$-alkylguanines generated by higher alkylating agents

As we had seen with MNNG, deletion of *atl1* increased the sensitivity of *S. pombe* to ENU but we were surprised to observe no impact on the sensitivity to BNNG or BzNU which generate the bulkier lesions, $O^6$-BuG and $O^6$-BnG in DNA. Furthermore, deletion of the TCR gene *rhp26*, which had no effect on sensitivity to MNNG or ENU, vastly increased sensitivity to BNNG and BzNU, while deletion of *swi10, rhp7, rhp23* and *rhp14* increased sensitivity to all of these alkylating agents (Figure 1A). For these bulkier lesions, the increased sensitivity in NER deletants was complemented by deletion of *atl1* and to a greater extent in the *rhp26* deletant. In addition, BzNU pulse treatment of G1-arrested WT cells resulted in a profound delay in DNA replication onset that was substantially shortened in the *atl1*-deletant. There were also increases in the length of the S-phase delay in *rhp26* and *swi10* deletants and again these were reduced by the additional deletion of *atl1,* the most extensive effect occurring in the *rhp26* deletant. These observations indicate that in the NER deletants, Atl1 binding to the bulkier $O^6$-alkylguanines leads to both transcription and replication blockage as shown in our model (Figure 7) and seen after very high doses of MNNG.

So why is there no phenotypic effect of *atl1* deletion? Given that the delay of replication onset was also observed in the *atl1* deletant, and all *alt1-NER* double deletants have shown increased sensitivity to the bulky agents, it is likely that, in the absence of Atl1, bulky $O^6$-alkylguanines can be processed by TCR or GGR, but less effectively, causing replication arrest, but without increased killing. In UV-irradiated *S. pombe* cells, bulky cyclobutane pyrimidine dimers (CPD) initiate TCR when they occupy the translocation site within the RNA pol II core subunit (Brueckner et al., 2007). Thus in the absence of Atl1, bulky $O^6$-

alkylguanines may mimic the effect of CPD. That *rad50* deletion significantly increased sensitivity of *atl1* deficient cells to BNNG and BzNU (Figure 1B) indicates that HR is involved in recovery from replication fork arrest and explains why the *atl1* deletant is not sensitive to bulky agents. The ability of BzNU to block replication explains why $O^6$-BnG appears to be ~20 times more toxic than $O^6$-MeG. Another consequence of this is that WT, *atl1* and other NER deletant cells progressing through S-phase become substantially more sensitive to killing by BZNU, but not MNNG (Figure S3).

In *E.coli* the ATL protein strongly enhances the repair of $O^6$-HOEt-, -1-hydroxypropyl- and -2-hydroxypropyl- guanine by NER (Mazon et al., 2009), and protects these adducts, but not $O^6$-MeG, against MMR-mediated toxicity (Mazon et al., 2010). This could also be explained by a high affinity of eATL for bulky $O^6$-alkylguanines and indicates functional similarity between the *S.pombe* and *E.coli* proteins.

## Atl1 complexes with DNA containing a variety of $O^6$-alkylguanines share common structures but different affinities

We sought to establish a biochemical basis for the effects of Atl1 by determination of its crystal structures and kinetic interaction characteristics with ODN containing different $O^6$-alkylguanines.

The crystal structures show, in all cases, that the alkylated base is flipped out of the helix and the DNA phosphodiester backbone undergoes a 45° bend. This remarkable similarity of the three-dimensional structures for all of the Atl1-DNA complexes suggests that neither the shape nor the extent of DNA helix distortion introduced by Atl1 can adequately explain ability of Atl1 to shuttle repair *via* different repair pathways for small and bulky $O^6$-alkylguanines. However, the Atl1 binding pocket can indeed accommodate a very wide variety of lesions, allowing numerous possibilities for interaction of the alkyl groups with amino acid residues in and around the binding pocket. Thus within the binding pocket, longer and bulkier groups make more hydrophobic interactions than smaller groups, or groups that can form weaker hydrogen bonds, potentially allowing tighter binding of the larger lesions.

Given the above observations, we used ELISA to determine equilibrium binding constants and SPR to measure the association and dissociation rates of the Atl1-DNA complexes and the corresponding dissociation constants. The ELISA results revealed similar and relatively low Atl1 affinity to ODN containing $O^6$-MeG and $O^6$-CMG and much higher affinities to substrates containing the other lesions, with $O^6$-EtG being intermediate. In SPR measurements, we found that the association ('on') rates for all ODN were very similar, but the rates of dissociation ("off" rates) for those containing $O^6$-MeG and $O^6$-CMG were more than one order of magnitude higher than those of ODN containing Pr, Bu, Bn, BT and Pob lesions. Overall, the dissociation constants ($K_D$) for this ODN series decreased in the order Me>CM>Et>HOEt>(Pr, Bu, Bn, BT, Pob) implying that the bulkiness of alkyl modification indeed determines the strength of Atl1 binding. We conclude that Atl1 forms more stable complexes with bulky $O^6$-alkylguanine residues: these results are consistent with the crystal structures and explain the phenotypes we have described.

## Model for the role of Atl1 in processing small and bulky $O^6$-alkylguanine lesions in DNA

Because Atl1 forms very similar structures with both small and bulky $O^6$-alkylguanines it is reasonable to suggest that any subsequent interactions with the downstream protein complexes rhp7/rhp16 and rhp41/rhp23, will also be identical, up to the point where Atl1 displacement from DNA takes place (Figure 7). Relatively facile dissociation of Atl1 from DNA containing small $O^6$-alkylguanines ($K_D$=0.5–0.91 nM) promotes accurate completion

of GGR, whereas strong Atl1 binding to bulky $O^6$-alkylguanines ($K_D$<0.1 nM) blocks GGR. When bulky $O^6$-alkylguanines are present in transcribed regions, Atl1, in complex with GGR damage recognition proteins, stalls the transcription machinery and diverts the damage to TCR, by activating Rhp26 and recruiting TFIIH and other downstream NER factors. In non-transcribed regions of the genome or in transcribed regions under circumstances where any of the NER factors are limited, the Atl1 complex will ultimately stall DNA replication complexes, leading to cell cycle arrest and/or cell death.

In conclusion, we provide evidence that the same DNA damage sensing protein can direct similar DNA lesions down different repair pathways according to the affinity for its substrates. For the tightly binding lesions, this might be considered a new branch of NER that fuses GGR to TCR.

Given the mechanistic similarities between ATL proteins and the mainly eukaryotic AGT proteins, these findings raise the question of whether or not $O^6$-alkylguanines that are poor substrates for the alkyl transfer function of AGTs might, by analogy, signal such lesions for repair by NER. Another possibility is that eukaryotes may possess a functional homologue of ATL that would provide an alternative mechanism for processing $O^6$-alkylguanines in DNA, a pathway that would have far-reaching clinical significance.

## EXPERIMENTAL PROCEDURES

### ODN syntheses

ODNs containing $O^6$-methylguanine ($O^6$-MeG) were obtained commercially (DNA Technology). The 23-mer sequence used was based on previous studies of the action of MGMT and Atl1 (Pearson et al., 2005) and was not based on the sequence of any known gene. ODNs containing, $O^6$- carboxymethyl (CM), -ethyl (Et), -hydroxyethyl (HOEt), -n-propyl (Pr), -n-butyl (Bu) -benzyl (Bn), -pyridyloxobutyl (Pob) and -4-bromothenyl (BT) guanine residues were synthesized by reaction of the appropriate alcohol during post-DNA synthesis chemistry as described (Millington et al., 2012; Shibata et al., 2006). All $O^6$-alkylguanine containing ODNs were purified by reversed phase HPLC (Millington et al., 2012; Shibata et al., 2006); confirmatory analysis was done by mass spectrometry (Shibata et al., 2006). The sequences of the various ODN used in these studies, and the positions of the modified bases (indicated by X) are given in Table S2. To produce duplexes, the ODN were annealed to complements with biotin or HEX at the 5′-end.

### Atl1 purification

For EMSA, ELISA and some SPR studies, Atl1 was expressed as an MBP-fusion protein from the pMAL-2c expression vector (New England Biolabs) construct as described by Pearson *et al.,* (2005, 2006) with minor modifications. MBP-Atl1 fusion protein (40 mg) was then cleaved with 0.1%w/v of Factor Xa (1 mg/mL, NEB); at room temperature for 2 hours. The efficiency of the reaction was assessed by resolving the cleavage products on a 15% SDS-polyacrylamide gel. The cleavage reaction was then applied to a Superdex200™ prep grade column (16 mm × 60 mm; GE Heathcare) that was pre-equilibrated with 50 mM Tris-HCl (pH 8.3), 100 mM NaCl. The column was eluted at a flow rate of 0.8 mL/min and 1.6 mL fractions were collected. Protein elution was monitored by absorption at 215 nm using a flow cell. Pooled Atl1 containing fractions were further purified through amylose columns to remove remaining uncleaved MBP-fusion protein.

### X-ray crystallography

For the XRC studies, C-terminally hexahistidine-tagged Atl1 was expressed and purified as described previously (Tubbs et al., 2009). Single-strand ODN of sequence 5′-

GCCATG**X**CTAGTA-3′, where **X**=$O^6$-HOEtG, $O^6$-PrG, $O^6$-BnG or $O^6$-CMG, were annealed with equimolar complementary ODN of sequence 5′-CTACTAGCCATGG-3′ to produce 13-mer double-strand DNA with a 5′-overhang on either end. This ODN was then mixed with purified Atl1 at an ODN:protein molar ratio of 1.5:1.

**Crystallization and X-ray Diffraction Data Collection—**Crystals were grown by the hanging drop vapor diffusion method mixing 1 μL of protein-DNA complex with 1 μL well solution.

Diffraction data for the Atl1:$O^6$-BnG-ODN complex were collected at SSRL beamline 11-1 at a wavelength of 0.97945 on a MAR325 detector. Diffraction data for the Atl1:$O^6$-HOEtG-ODN, Atl1:$O^6$-PrG-ODN, and Atl1:$O^6$-CMG-ODN complexes were collected at ALS beamline 12.3.1 at a wavelength of 1.1158 Å on an ADSC Q315 detector. Diffraction data were processed with HKL2000 (Otwinowski and Minor, 1997). Structures were solved by molecular replacement with Phaser (McCoy et al., 2007), using the Atl1 structure (pdb 3GVA) as a search model for Atl1–DNA complexes.

**Crystallographic Structure Refinement and Analysis—**Crystallographic refinement was done with ***P****ython-based* ***H****ierarchical* ***EN****vironment for* ***I****ntegrated* ***X****tallography* (PHENIX) (Adams et al., 2010). Coot was used for manual model building into $2F_o - F_c$ and composite omit and simulated annealing omit $2F_o - F_c$ and $F_o - F_c$ electron density maps (Emsley and Cowtan, 2004). DNA was built into the model after two rounds of refinement. Water molecules were added to regions of greater than 3σ in a $F_o - F_c$ difference map after two rounds of refinement. Structural superimpositions were done with Sequoia (Bruns et al., 1999). Structure figures were made with PyMol (http://www.pymol.org).

## EMSA methodology

ODNs were annealed by mixing equimolar amounts of $O^6$-alkylguanine-containing ODN and complement that was fluorescently labeled at the 5′-end with HEX, in 500 mM NaCl, heating in a dry-block at 80°C for 5 min, then allowing to cool to room temperature. Aliquots of the ODN were incubated with Atl1 (5 uL of 1pmole/uL) in total volume of 20 μL of buffer I (50 mM Tris-HCl, 1 mM EDTA, 3 mM dithiothreitol, pH 8.3) for 1 hour at 37°C and then subjected to non-denaturing gel electrophoresis (15% acrylamide) in TBE buffer (89 mM Tris-HCl, 89 mM boric acid, 2 mM EDTA) at 100V for 2 hours. Gels were scanned using the HEX settings on a Pharos laser scanner (BioRad). Additional EMSA controls included incubation with the non-DNA binding protein MBP (5 uL of 1pmole/uL in 20 μL buffer I) and incubation of Atl1, MBP or the ODN incubation mixes with amounts of proteinase K (Sigma; 2 ul of a 10 ug/mL solution in water) that had been shown to degrade the amounts of the individual proteins used. The presence of the Atl1 and MBP proteins and their degradation by PK was shown by electrophoretic transfer of the bands to nitrocellulose membranes (GE healthcare) at 100V for 1 hour and probing with anti-Atl1 rabbit polyclonal antiserum that we had generated to purified recombinant Atl1 or anti-MBP antibodies (New England Biolab) followed by incubation with horseradish peroxidase-labeled anti-rabbit antibodies (DakoCytomation) and detection by enhanced chemiluminescence (GE Healthcare).

## Direct ELISA methodology

$O^6$-alkylguanine-containing ODNs were annealed to the biotinylated complement, immobilized on streptavidin (SA) coated 96-well plates and incubated with incrementally increasing concentrations of Atl1. Following sequential 1-hour room temperature incubations with anti-Atl1 antibodies, goat anti rabbit HRP was added and binding

quantified by measurement of chemiluminescence on a TECAN GENios plate-reader. Binding was expressed as % of ODN bound. Binding curves were plotted and $K_D$ values *i.e.* the concentration of Atl1 (nM) at which 50% of the target ODN is bound, determined.

### Yeast strains, media and standard genetic methods

The genotypes of *S. pombe* strains used in this study are listed in Table S1. The majority of strains used in this study originated from GM1 (Pearson et al., 2006). The disruptions of the *rhp7*, *rhp26* and *rad23* genes in GM1 strain were done by one step PCR-based gene targeting (Bahler et al., 1998; Longtine et al., 1998).

The standard media and general methods were as described (Gutz et al., 1974; Moreno et al., 1991). Yeast extract agar (YEA) contained 0.5% Difco yeast extract, 3% glucose, 1.8% agar; yeast extract liquid (YEL) - 0.5% Difco yeast extract and 3% glucose. Adenine, leucine, uracil, histidine, lysine (100 mg/l each) were added to YEA/YEL where required.

### Agar plate ("spot") assays

YEA plates were prepared by adding the appropriate volume of stock solutions of different alkylating agents (100 mg/mL in dry DMSO) to cooled molten agar. Serial 1 in 10 dilutions of *S. pombe* cultures containing $5 \times 10^7$ cells/mL were spotted on YEA plates (5 μl per spot). Photographs were taken after 4–5 days of incubation at 30°C for cdc10+ strains and 25°C for *cdc10-M17* mutants.

### Determination of MNNG sensitivity by clonogenic survival assay

To determine MNNG sensitivity, yeast cells were streaked to single colonies on YEA plates and grown for 4–5 days. Suspensions of cells derived from a single colony ($10^7$ cell/mL) were exposed to different concentrations of MNNG for 10 min in YEL then diluted 100-fold in distilled water to stop the reaction. Serial cell dilutions were then plated in YEA medium to attain growth of approximately 200 colonies per plate. Cell titer was estimated by plating the original cell suspension without MNNG treatment. After 7 days of growth at 30°C, cell survival (%) was calculated as ratio between the number of colonies and the number of cells plated.

### SPR analyses

The interaction of Atl1 with ODN containing $O^6$-Me, $O^6$-CM, $O^6$-Et, $O^6$-HOEt, $O^6$-Pr, $O^6$-Bu, $O^6$-Bn, $O^6$-Pob and $O^6$- BT guanine and guanine-containing control ODN (Table S2) were analysed using Bio-Rad ProteOn "XPR36" SPR system and neutravidin-coated NLC sensor chips. Proteon Manager software was used to fit the binding curves and calculate the binding constants and data were presented in the form of "on" ($k_a$) and "off" ($k_d$) rates and dissociation constants ($K_D$).

### Analysis of S-phase progression by FACS analysis

*Cdc10-M17* cells were synchronized in G1-S by incubation at 37°C for 4 h (Kim and Huberman, 2001); then treated with MNNG or BZNU for 10 min and shifted to 25°C. At 20 min intervals, aliquots of cells (100 μl) were taken for flow cytometry analysis. Samples for FACS were prepared as described previously (Doll et al., 2005; Kim and Huberman, 2001) with minor modifications. S-phase progression was assessed using FlowJo software as described (Willis and Rhind, 2009). The DNA peak position for the zero time sample was used to set the 1C value (pre-replication) and the 2C value (post replication) was set from the location of the DNA peak in the late time points for the untreated control samples. For each time point, S-phase progression was quantitated using the equation: % progression = (C − A)/(B − A), where A = 1C, B = 2C, and C = mean values for S-phase peaks.

### Determination of $O^6$-MeG and $O^6$-BnG levels in *S. pombe* cells after treatment with MNNG and BzNU

*S. pombe* cells were grown in YEL to an $OD_{600}$ of 0.5 and treated with 120 and 240 μg/mL MNNG for 10 minutes at 30°C. Treatment with 1 mg/mL BzNU for 60 and 90 min was in TE, pH 8.1 to increase BZNU hydrolysis. Cells were then centrifuged (800 × g for 2 minutes) and resuspended in the same volume of TE, pH 8.1. After treatment with MNNG and BzNU, cells were harvested by centrifugation as above and snap frozen in dry ice. DNA was isolated by phenol extraction and ethanol precipitation. $O^6$-MeG and $O^6$-BnG in DNA were quantified using a modification of the standard MGMT activity assay procedure as described previously (Watson and Margison, 2000; Watson et al., 2009).

## Supplementary Material

Refer to Web version on PubMed Central for supplementary material.

## Acknowledgments

This work was supported by Cancer Research UK, National Institutes of Health grant CA097209 (JAT), the Skaggs Institute for Chemical Biology (JLT), EPSRC (CLM), BBSRC (OJW, DMW), CHEMORES (GPM), and the Royal Thai Government (PS).

X-ray diffraction technologies at the SIBYLS beamline 12.3.1 at the Advanced Light Source, Lawrence Berkeley National Laboratory, are supported by the U.S. Department of Energy (DOE) program Integrated Diffraction Analysis Technologies (IDAT). Diffraction data collection at the Stanford Synchrotron Radiation Light source is supported by DOE and NIH.

We acknowledge the help of Dr. Jonathan Popplewell of Bio-Rad Laboratories in the analysis of SPR data and Grant Guenther and Matthew Kroeger for purifying the Atl1 protein used for crystallographic studies.

## References

Adams PD, Afonine PV, Bunkoczi G, Chen VB, Davis IW, Echols N, Headd JJ, Hung LW, Kapral GJ, Grosse-Kunstleve RW, et al. PHENIX: a comprehensive Python-based system for macromolecular structure solution. Acta Crystallogr D Biol Crystallogr. 2010; 66:213–221. [PubMed: 20124702]

Bahler J, Wu JQ, Longtine MS, Shah NG, McKenzie A III, Steever AB, Wach A, Philippsen P, Pringle JR. Heterologous modules for efficient and versatile PCR-based gene targeting in Schizosaccharomyces pombe. Yeast. 1998; 14:943–951. [PubMed: 9717240]

Beranek DT. Distribution of methyl and ethyl adducts following alkylation with monofunctional alkylating agents. Mutat Res. 1990; 231:11–30. [PubMed: 2195323]

Brueckner F, Hennecke U, Carell T, Cramer P. CPD damage recognition by transcribing RNA polymerase II. Science. 2007; 315:859–862. [PubMed: 17290000]

Bruns CM, Hubatsch I, Ridderstrom M, Mannervik B, Tainer JA. Human glutathione transferase A4-4 crystal structures and mutagenesis reveal the basis of high catalytic efficiency with toxic lipid peroxidation products. J Mol Biol. 1999; 288:427–439. [PubMed: 10329152]

den Dulk B, van Eijk P, de Ruijter M, Brandsma JA, Brouwer J. The NER protein Rad33 shows functional homology to human Centrin2 and is involved in modification of Rad4. DNA Repair (Amst). 2008; 7:858–868. [PubMed: 18387345]

Doll E, Molnar M, Hiraoka Y, Kohli J. Characterization of rec15, an early meiotic recombination gene in Schizosaccharomyces pombe. Curr Genet. 2005; 48:323–333. [PubMed: 16252089]

Emsley P, Cowtan K. Coot: model-building tools for molecular graphics. Acta Crystallogr D Biol Crystallogr. 2004; 60:2126–2132. [PubMed: 15572765]

Fousteri M, Mullenders LH. Transcription-coupled nucleotide excision repair in mammalian cells: molecular mechanisms and biological effects. Cell Res. 2008; 18:73–84. [PubMed: 18166977]

Fuss JO, Tainer JA. XPB and XPD helicases in TFIIH orchestrate DNA duplex opening and damage verification to coordinate repair with transcription and cell cycle via CAK kinase. DNA Repair (Amst). 2011; 10:697–713. [PubMed: 21571596]

Gutz, H.; Heslot, H.; Leupold, U.; Loprieno, N. Handbook of genetics. King, RC., editor. Vol. 1. NY: Plenum Press; 1974. p. 395-446.

Hickman MJ, Samson LD. Apoptotic Signaling in Response to a Single Type of DNA Lesion, $O^6$-Methylguanine. Molecular cell. 2004; 14:105–116. [PubMed: 15068807]

Kim SM, Huberman JA. Regulation of replication timing in fission yeast. Embo J. 2001; 20:6115–6126. [PubMed: 11689451]

Lombaerts M, Goeloe JI, den Dulk H, Brandsma JA, Brouwer J. Identification and characterization of the rhp23(+) DNA repair gene in Schizosaccharomyces pombe. Biochem Biophys Res Commun. 2000; 268:210–215. [PubMed: 10652237]

Lombaerts M, Peltola PH, Visse R, den Dulk H, Brandsma JA, Brouwer J. Characterization of the rhp7(+) and rhp16(+) genes in Schizosaccharomyces pombe. Nucleic Acids Res. 1999; 27:3410–3416. [PubMed: 10446227]

Longtine MS, McKenzie A III, Demarini DJ, Shah NG, Wach A, Brachat A, Philippsen P, Pringle JR. Additional modules for versatile and economical PCR-based gene deletion and modification in Saccharomyces cerevisiae. Yeast. 1998; 14:953–961. [PubMed: 9717241]

Margison GP, Butt A, Pearson SJ, Wharton S, Watson AJ, Marriott A, Caetano CM, Hollins JJ, Rukazenkova N, Begum G, Santibanez-Koref MF. Alkyltransferase-like proteins. DNA Repair (Amst). 2007; 6:1222–1228. [PubMed: 17500045]

Margison GP, Povey AC, Kaina B, Santibanez Koref MF. Variability and regulation of $O^6$-alkylguanine-DNA alkyltransferase. Carcinogenesis. 2003; 24:625–635. [PubMed: 12727789]

Margison GP, Santibanez Koref MF, Povey AC. Mechanisms of carcinogenicity/chemotherapy by $O^6$-methylguanine. Mutagenesis. 2002; 17:483–487. [PubMed: 12435845]

Marti TM, Kunz C, Fleck O. Repair of damaged and mismatched DNA by the XPC homologues Rhp41 and Rhp42 of fission yeast. Genetics. 2003; 164:457–467. [PubMed: 12807767]

Mazon G, Philippin G, Cadet J, Gasparutto D, Fuchs RP. The alkyltransferase-like ybaZ gene product enhances nucleotide excision repair of O(6)-alkylguanine adducts in E. coli. DNA Repair (Amst). 2009; 8:697–703. [PubMed: 19269902]

Mazon G, Philippin G, Cadet J, Gasparutto D, Modesti M, Fuchs RP. Alkyltransferase-like protein (eATL) prevents mismatch repair-mediated toxicity induced by $O^6$-alkylguanine adducts in Escherichia coli. Proc Natl Acad Sci U S A. 2010; 107:18050–18055. [PubMed: 20921378]

McCoy AJ, Grosse-Kunstleve RW, Adams PD, Winn MD, Storoni LC, Read RJ. Phaser crystallographic software. J Appl Crystallogr. 2007; 40:658–674. [PubMed: 19461840]

Millington CL, Watson AJ, Marriott AS, Margison GP, Povey AC, Williams DM. Convenient and efficient syntheses of oligodeoxyribonucleotides containing $O^6$-(carboxymethyl)guanine and $O_6$-(4-oxo-4-(3-pyridyl)butyl)guanine. Nucleosides Nucleotides Nucleic Acids. 2012; 31:328–338. [PubMed: 22444194]

Min JH, Pavletich NP. Recognition of DNA damage by the Rad4 nucleotide excision repair protein. Nature. 2007; 449:570–575. [PubMed: 17882165]

Moreno S, Klar A, Nurse P. Molecular genetic analysis of fission yeast Schizosaccharomyces pombe. Methods Enzymol. 1991; 194:795–823. [PubMed: 2005825]

Nouspikel T. DNA repair in mammalian cells: Nucleotide excision repair: variations on versatility. Cell Mol Life Sci. 2009; 66:994–1009. [PubMed: 19153657]

Otwinowski Z, Minor W. Processing of X-ray Diffraction Data Collected in Oscillation Mode. Methods Enzymol. 1997; 276:307–326.

Paoletti A, Bordes N, Haddad R, Schwartz CL, Chang F, Bornens M. Fission yeast cdc31p is a component of the half-bridge and controls SPB duplication. Mol Biol Cell. 2003; 14:2793–2808. [PubMed: 12857865]

Pearson SJ, Ferguson J, Santibanez-Koref M, Margison GP. Inhibition of $O^6$-methylguanine-DNA methyltransferase by an alkyltransferase-like protein from Escherichia coli. Nucleic Acids Res. 2005; 33:3837–3844. [PubMed: 16027108]

Pearson SJ, Wharton S, Watson AJ, Begum G, Butt A, Glynn N, Williams DM, Shibata T, Santibanez-Koref MF, Margison GP. A novel DNA damage recognition protein in Schizosaccharomyces pombe. Nucleic Acids Res. 2006; 34:2347–2354. [PubMed: 16679453]

Prakash S, Prakash L. Nucleotide excision repair in yeast. Mutat Res. 2000; 451:13–24. [PubMed: 10915862]

Reed SH. Nucleotide excision repair in chromatin: Damage removal at the drop of a HAT. DNA Repair (Amst). 2011; 10:734–742. [PubMed: 21600858]

Shibata T, Glynn N, McMurry TB, McElhinney RS, Margison GP, Williams DM. Novel synthesis of $O^6$-alkylguanine containing oligodeoxyribonucleotides as substrates for the human DNA repair protein, $O_6$-methylguanine DNA methyltransferase (MGMT). Nucleic Acids Res. 2006; 34:1884–1891. [PubMed: 16609128]

Singer, B.; Grunberger, D. Molecular Biology of Mutagens and Carcinogens. New York: Plenum Press; 1983.

Tubbs JL, Latypov V, Kanugula S, Butt A, Melikishvili M, Kraehenbuehl R, Fleck O, Marriott A, Watson AJ, Verbeek B, et al. Flipping of alkylated DNA damage bridges base and nucleotide excision repair. Nature. 2009; 459:808–813. [PubMed: 19516334]

Watson AJ, Margison GP. $O^6$-alkylguanine-DNA alkyltransferase assay. Methods Mol Biol. 2000; 152:49–61. [PubMed: 10957968]

Watson AJ, Middleton MR, McGown G, Thorncroft M, Ranson M, Hersey P, McArthur G, Davis ID, Thomson D, Beith J, et al. O(6)-methylguanine-DNA methyltransferase depletion and DNA damage in patients with melanoma treated with temozolomide alone or with lomeguatrib. Br J Cancer. 2009; 100:1250–1256. [PubMed: 19367283]

Willis N, Rhind N. Mus81, Rhp51(Rad51), and Rqh1 form an epistatic pathway required for the S-phase DNA damage checkpoint. Mol Biol Cell. 2009; 20:819–833. [PubMed: 19037101]

Yasuhira S, Morimyo M, Yasui A. Transcription dependence and the roles of two excision repair pathways for UV damage in fission yeast Schizosaccharomyces pombe. J Biol Chem. 1999; 274:26822–26827. [PubMed: 10480889]

## Highlights

- Atl1 binds to and forms similar structures with a wide range of $O^6$-alkylguanines
- Relatively weak Atl1 binding to simple lesions initiates GGR
- Strong binding to more complex lesions activates TCR and stalls DNA replication

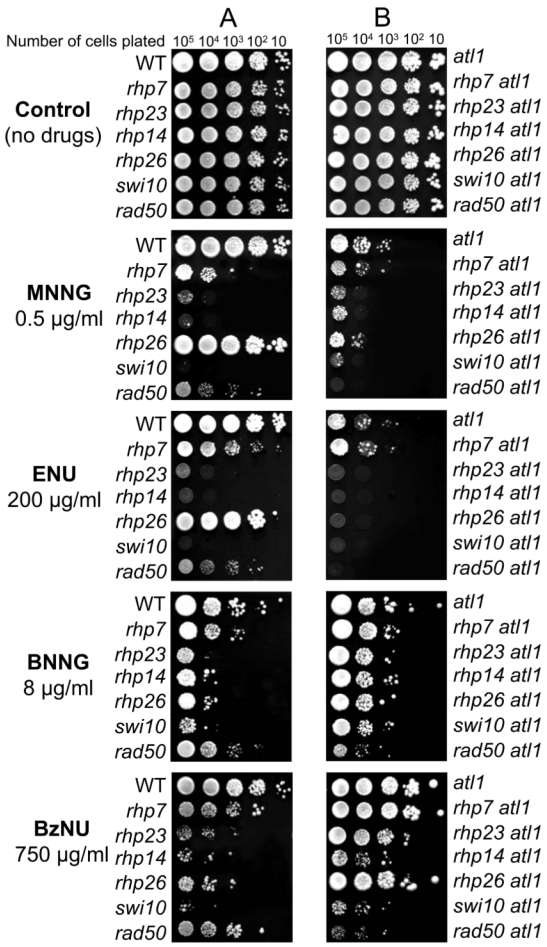


**Figure 1. Agar plate ("spot") assays for *atl1*-, NER- and HR - deficient mutants after treatment with MNNG, ENU, BNNG and BzNU**

(A) Sensitivity of WT strain (GM1) and single deletants of *rhp7* (GM56), *rhp23* (GM50), *rhp14* (GM25), *rhp26* (GM51), *swi10* (OL455) and *rad50* (GM11)

(B) Sensitivity of *atl1* single (GM3) and the double deletants: *atl1 rhp7* (GM61), *atl1 rhp23* (GM100), *atl1 rhp14* (GM32), *atl1 rhp26* (GM60), *atl1 swi10* (GM48) and *atl1 rad50* (GM +15). See also Figure S1.

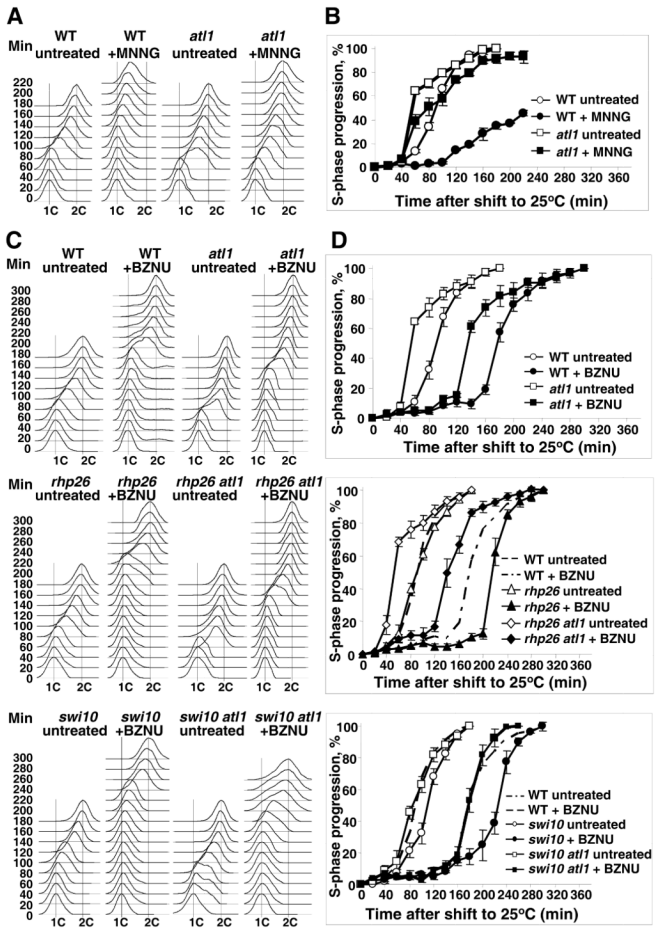


**Figure 2. Survival of WT and deletant *S. pombe* strains and persistence of $O^6$-MeG in DNA after exposure to MNNG**

(A–F) MNNG-sensitivity measured by clonogenic survival assays for WT (GM1) and deletants: *atl1* (GM3)

(A) *swi10* (OL455), *atl1 swi10* (GM48)

(B) *rhp7* (GM56), *atl1 rhp7* (GM61)

(C) *rhp23* (GM50), *atl1 rhp23* (GM100)

(D) *rhp41* (TM4), *atl1 rhp41* (GM46)

(E) *rhp26* (GM51), *rhp7* (GM56), *rhp7 rhp26* (GM121)

(F) *rad50* (GM11), *atl1 rad50* (GM15)

(G) The amount of $O^6$-MeG in DNA at various times after 10 min exposure to MNNG (10 μg/mL).

Values are the mean of triplicate or quadruplicate treatments and error bars represent standard error of the mean.

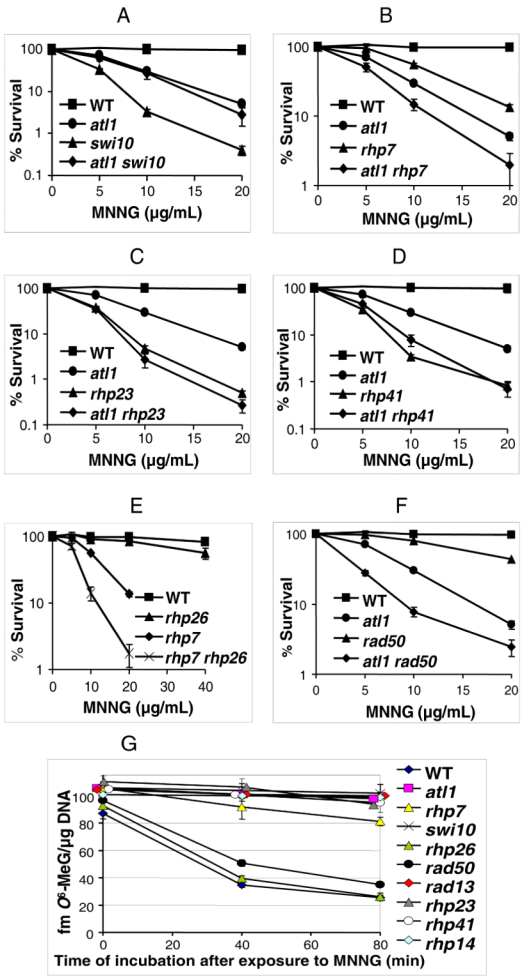


**Figure 3. Flow cytometric quantitation of S-phase progression after MNNG and BzNU treatment**

*Cdc10-M17* cells grown at 25°C and synchronized in G1 by shifting to 37°C for 4.5 hours. Before release from arrest, cells were treated with BNNG or MNNG (10 min), centrifuged and resuspended in YEL. Samples were taken every 20 min and nuclear DNA content was measured by flow cytometry.

(A) Overlays of S-phase flow cytometry histogram stacks and

(B) S-phase progression after treatment with high concentrations of MNNG leading to ~0.5% cell survival. S-phase progression (%) was measured by the relative shifting of the mean of S-phase peaks from unreplicated 1C toward fully replicated 2C values preset as 0% and 100% respectively.

(C) Overlays of S-phase flow cytometry histogram stacks and

(D) S-phase progression comparing WT (SP413), *atl1* (GM62), *rhp26* (GM106), *rhp26 atl1* (GM107), *swi10* (GM108), *swi10 atl1* (GM109) strains after treatment with BzNU (0.5 mg/mL). Values are the mean of triplicate experiments and error bars represent SEM. The values of cell survival were as follows: wild-type (27%), *atl1* (32.7%), *rhp26* (13%), *rhp26 atl1* (17.5%), s*wi10* (8.8%), *swi10 atl1* (25.8%). See also Figure S3.

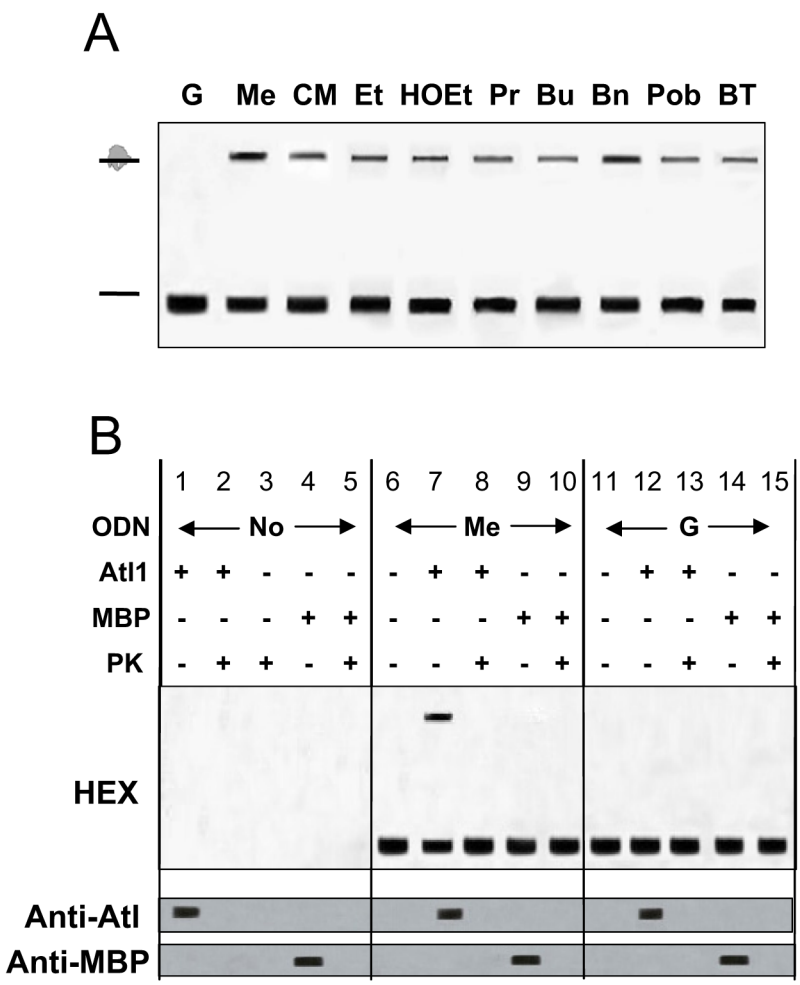


**Figure 4. Qualitative assessment of the binding of Atl1 to ODN by EMSA**

(A) Atl1 binds specifically to ODNs containing $O^6$-alkylguanines.
ODNs were annealed by mixing complement (5′-[HEX]-GGGCCAGCACGGAGCTGCAGTTC) with the "lesion"-containing ODN (5′-GAACTXCAGCTCCGTGCTGGCCC, where X is guanine (G) or the modified bases: $O^6$-methyl (Me), -carboxymethyl (CM), -ethyl (Et), -hydroxyethyl (HOEt), -n-propyl (Pr), -butyl (Bu) -benzyl (Bn), -pyridyloxobutyl (Pob) and -4-bromothenyl (BT). Atl1 (5 μM) was incubated with duplex ODN (1 μM) in total volume of 10 μL of reaction buffer then electrophoresed. Gels were scanned using a Pharos laser scanner (BioRad).
(B) Additional EMSA controls for $O^6$-MeG-containing ODN which include incubation with the non-DNA binding protein MBP and incubation of Atl1, MBP or the ODN incubation mixes with proteinase K (PK). The upper gel photograph was obtained a Pharos laser scanner and the gel was electroblotted to nitrocellulose. The Atl1 (centre gel photograph) and MBP proteins (lower gel photograph) and their degradation by PK were visualized by western blot with rabbit anti-Atl1 polyclonal antiserum or anti-MBP antibodies followed by incubation with horseradish peroxidase-labeled anti-rabbit antibodies and detection by enhanced chemiluminescence. Data for all other ODNs are shown in Figure S4.

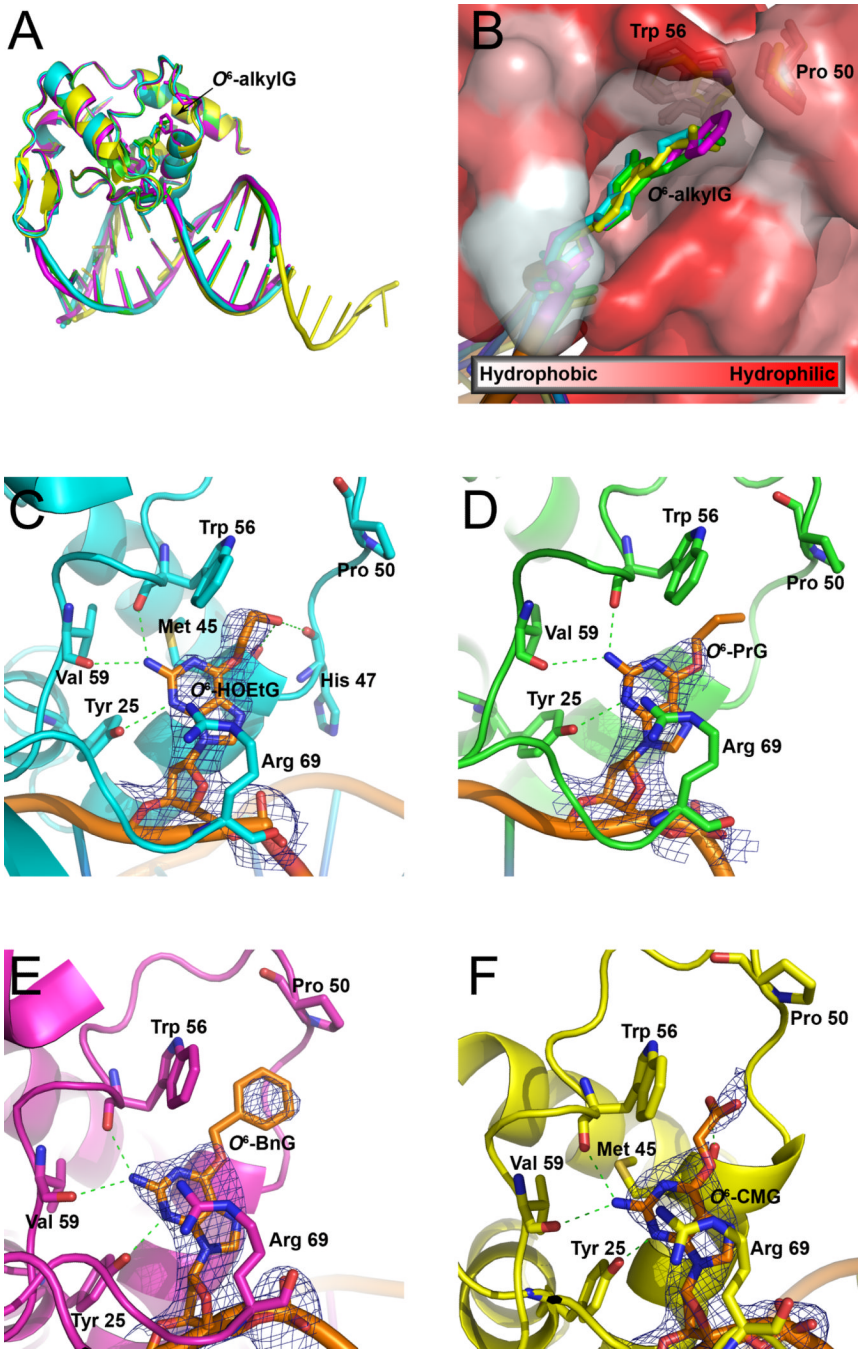


**Figure 5. Crystal structures for Atl1 in complex with ODN containing $O^6$-HOEtG (cyan) $O^6$-PrG (green), $O^6$-BnG (magenta), or $O^6$-CMG (yellow)**

(A) Structural overlay of Atl1:ODN complexes showing similar DNA bend.

(B) Molecular surface of Atl1 lesion-binding pocket colored by hydrophobicity (white=most hydrophobic; red=least hydrophobic) and overlaid with Atl1:ODN complex structures. Trp 56 and Pro 50 are shown for reference.

(C–F) Binding of $O^6$-HOEtG (C), $O^6$-PrG (D), $O^6$-BnG (E), and $O^6$-CMG (F) within the Atl1 binding pocket. $2F_o$-$F_c$ omit electron density (blue) is shown for each $O^6$-alkylG adduct (orange). Hydrogen bonds are shown as dashed green lines. The accompanying crystallographic data are listed in Table 1.

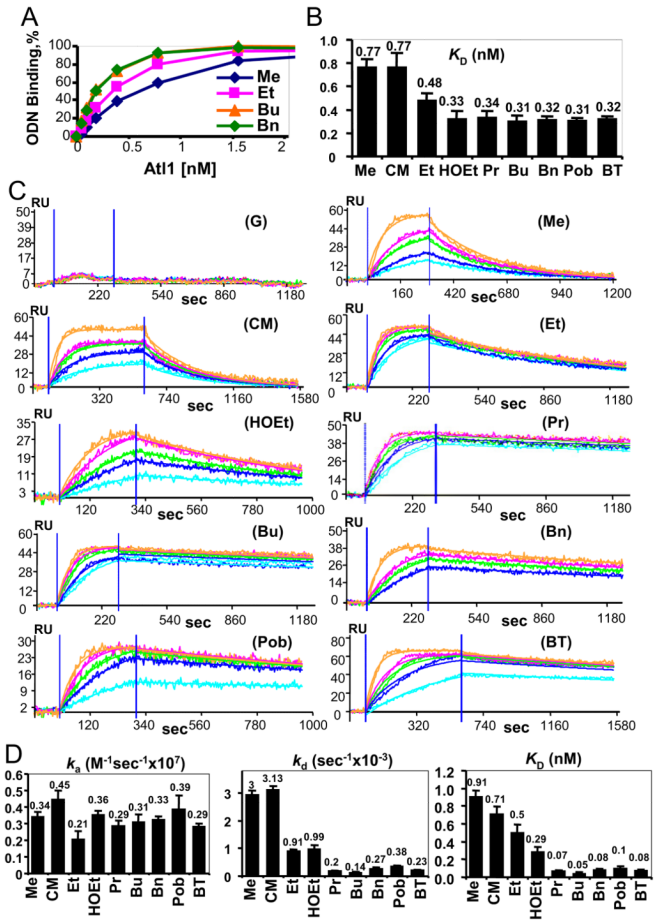


**Figure 6. Quantitative assessment of the binding of Atl1 to ODN by ELISA and SPR**

(A) Direct ELISA: effect of incubation of increasing concentrations of Atl1 with ODN duplexes bound via 5′-terminal biotin to SA-coated plates; typical binding curves.

(B) $IC_{50}$ values extrapolated from the direct ELISA curves.

(C) SPR sensograms for the indicated ODN.

(D) SPR-determined interaction constants $k_a$ (association 'on' rate), $k_d$ (dissociation rate) and $K_D$ (dissociation constant). Values are means of at least triplicate determinations and error bars indicate standard error of the mean.

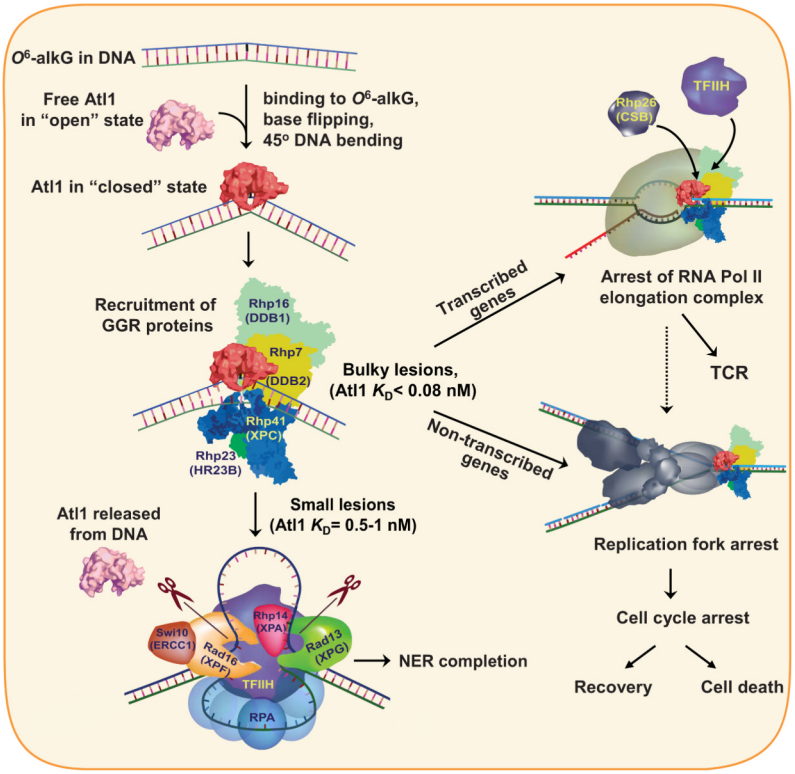


**Figure 7. Schematic representation of the role of Atl1 in repair of $O^6$-alkylguanines**

Atl1 binding to small $O^6$-alkylguanine modifications activates GGR whereas bulky $O^6$-alkylguanines engage both GGR and TCR, block chromosomal replication and invoke cell cycle arrest or cell death.

## Table 1

X-ray Crystallography Data Collection and Refinement Statistics

| | $O^6$-HOEtG | $O^6$-PrG | $O^6$-BnG | $O^6$-CMG |
|---|---|---|---|---|
| **Data collection** | | | | |
| Space group | $P6_122$ | $P6_122$ | $P6_122$ | $P4_12_12$ |
| Cell dimensions | | | | |
| *a*, *b*, *c* (Å) | 59.8, 59.8, 232.7 | 59.5, 59.5, 236.9 | 59.9, 59.9, 237.1 | 85.2, 85.2, 150.7 |
| αβγ (°) | 90, 90, 120 | 90, 90, 120 | 90, 90, 120 | 90, 90, 90 |
| Resolution (Å) | 50.0-3.10 (3.21-3.10) | 50.0-3.05 (3.16-3.05) | 50.0-2.84 (2.94-2.84) | 50.0-2.85 (2.95-2.85) |
| $R_{sym}$ | 6.5 (51.6) | 5.0 (34.9) | 9.0 (45.9) | 6.2 (49.9) |
| $I/\sigma I$ | 49.0 (2.2) | 59.5 (2.7) | 22.8 (2.1) | 31.2 (1.9) |
| Completeness (%) | 97.1 (77.5) | 97.6 (82.3) | 93.0 (61.1) | 95.6 (77.0) |
| Redundancy | 14.0 | 15.2 | 10.1 | 6.7 |
| **Refinement** | | | | |
| Resolution (Å) | 38.7-3.10 | 34.8-3.05 | 39.0-2.84 | 43.3 - 2.85 |
| No. reflections | 4488 | 4797 | 5915 | 11727 |
| $R_{work}/R_{free}$ | 22.5/28.3 | 25.0/29.5 | 17.3/25.3 | 22.0/28.2 |
| No. atoms | | | | |
| Protein | 891 | 898 | 891 | 1782 |
| Ligand/ion | 530 | 530 | 534 | 1076 |
| Water | 4 | 1 | 0 | 0 |
| *B*-factors | | | | |
| Protein | 147.0 | 139.5 | 105.9 | 122.6 |
| Ligand/ion | 137.1 | 126.2 | 113.6 | 126.6 |
| Water | 98.8 | 88.79 | N/A | N/A |
| R.m.s. deviations | | | | |
| Bond lengths (Å) | 0.010 | 0.010 | 0.008 | 0.011 |
| Bond angles (°) | 1.6 | 1.6 | 1.3 | 2.0 |

One crystal was used for each dataset. Values in parentheses are for highest-resolution shell.